Eur. Phys. J. D (2022) 76:218
https://doi.org/10.1140/epjd/s10053-022-00549-6

THE EUROPEAN PHYSICAL JOURNAL D

Regular Article – Cold Matter and Quantum Gases

Bichromatic state-dependent disordered potential for Anderson localization of ultracold atoms

Baptiste Lecoutre, Yukun Guo, Xudong Yu, M. Niranjan, Musawwadah Mukhtar, Valentin V. Volchkov, Alain Aspect, and Vincent Josse[a]

Université Paris-Saclay, Institut d'Optique Graduate School, CNRS, Laboratoire Charles Fabry, 91127 Palaiseau, France

Received 21 July 2022 / Accepted 27 October 2022 / Published online 17 November 2022

Abstract. The ability to load ultracold atoms at a well-defined energy in a disordered potential is a crucial tool to study quantum transport, and in particular Anderson localization. In this paper, we present a new method for achieving that goal by rf transfer of atoms in an atomic Bose-Einstein condensate from a disorder-insensitive state to a disorder-sensitive state. It is based on a bichromatic laser speckle pattern, produced by two lasers whose frequencies are chosen so that their light-shifts cancel each other in the first state and add up in the second state. Moreover, the spontaneous scattering rate in the disorder-sensitive state is low enough to allow for long observation times of quantum transport in that state. We theoretically and experimentally study the characteristics of the resulting potential.

1 Introduction

Ultracold atoms offer remarkable quantum simulators to experimentally study difficult condensed-matter problems [1]. Quantum transport and Anderson localization have been directly observed by launching atoms in disordered potentials produced by far off-resonance laser speckle [2–8]. Convincing results with quantitative comparison to calculations have been obtained on Anderson localization in 1D speckle disordered potentials [2,3,9], and on direct signature of weak localization phenomena [4,5,10]. When it comes to 3D Anderson localization, several observations have been reported [6–8], but precise quantitative measurements are still lacking. The reason is that in experiments performed so far, atoms launched in the disorder have a large energy dispersion so that evaluating the mobility edge demands a deconvolution leading to large uncertainties.

It would thus be extremely interesting to have a method to launch atoms in the disorder at a precisely defined energy. By scanning the energy around the mobility edge, it would allow one to determine precisely the mobility edge. One might even evaluate critical exponents. Note that, there is no exact theory yielding the value of both quantities [11,12], and it is thus highly desirable to compare the results of approximate theoretical treatments [13–16] or numerical results [17–19] with experimental results. Among other experiments that would benefit from such an improved control of the energy of the atoms launched in the disorder, one can cite measurements of spectral functions [20], tests of the landscape theory of localization [21], search for sophisticated signatures of localization [22–26], or even the study of 2D localization [27,28].

Our strategy for launching atoms with a precisely defined energy (see Fig. 1) consists in performing a rf transition from a state insensitive to disorder (state $|1\rangle$) to a state sensitive to disorder (state $|2\rangle$). The energy of the populated eigenstates in the disorder can be adjusted by the control of the frequency of the rf. In the disorder, the atom energy levels form a continuum. Since the initial state is discrete, a priori one has a one-way transition characterized by a rate Γ given by the Fermi Golden Rule, which also sets the minimum energy dispersion of the transferred atoms. For an interaction time t_{rf} shorter than Γ^{-1}, as in the experiment reported below, the energy dispersion of the arrival states, i.e., of the atoms transferred to the continuum, is Fourier-limited and given by $\Delta E = \hbar/t_{\mathrm{rf}}$.

A first implementation of that scheme was demonstrated in the work of Volchkov et al. [20], where we used a rf atom transfer between states with different sensitivities to a monochromatic laser speckle disorder. These different sensitivities stemmed from the very different detunings of the laser are used to produce the disorder, for the initial state $|1\rangle$ and the final state $|2\rangle$ (see Fig. 2). The narrow Fourier-limited energy distribution we obtained—two orders of magnitude lower than in previous experiments [18,20]—allowed us to make a quantitative study of the spectral function of the atoms in that disorder, exploring different regimes of quantum transport from the *quantum* low disorder regime to the *classical* strong disorder regime [29–31].

[a] e-mail: vincent.josse@universite-paris-saclay.fr (corresponding author)

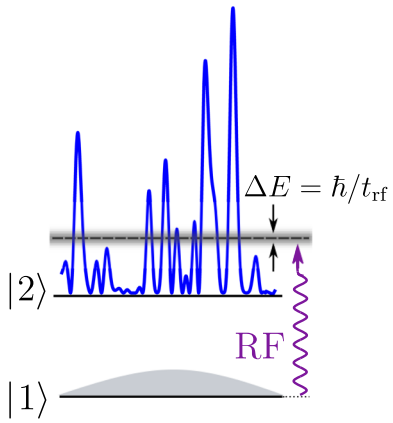

Fig. 1 Launching atoms at a well-defined energy in a disordered potential. It consists of transferring atoms of a Bose-Einstein condensate from the discrete, disorder-insensitive state $|1\rangle$ with a well-defined energy, to a state $|2\rangle$ sensitive to disorder, thus belonging to a continuum. By tuning the rf transfer frequency $\omega_{\rm rf}$, one can select the mean energy of the atoms transferred in $|2\rangle$, while adjusting the rf power and duration of the transfer allows one to control the spread in energy ΔE of the transferred atoms.

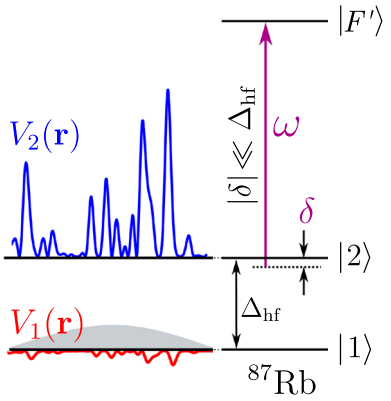

Fig. 2 State-dependent disorder in a monochromatic speckle. The laser at frequency ω is closer to resonance for the $|2\rangle \rightarrow |F'\rangle$ transition than for the $|1\rangle \rightarrow |F'\rangle$ transition. The light shift induced in $|2\rangle$ is thus larger than the light shift induced in $|1\rangle$, and for a speckle induced by that laser, the resulting disorder is stronger in $|2\rangle$. In the figure, corresponding to a blue detuned laser, the disorder in $|2\rangle$ is repulsive and is limited below. For a detuning δ of opposite sign (red detuned laser), the disorder would be attractive in $|2\rangle$, and limited above. The drawback of that method is the large spontaneous scattering of laser photons in state $|2\rangle$, resulting in a loss of coherence for the quantum transport of atoms in state $|2\rangle$.

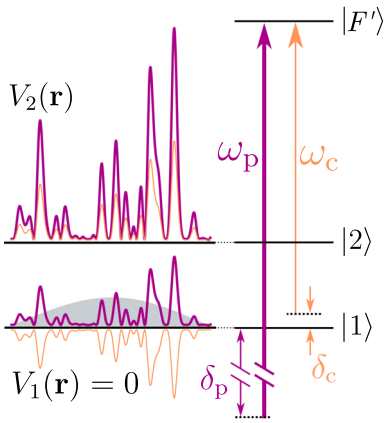

Fig. 3 State-dependent disorder in a bichromatic speckle. The two lasers at frequencies $\omega_{\rm p}$ (principal) and $\omega_{\rm c}$ (compensation) create disordered potentials that add up in $|2\rangle$ but cancel each other in $|1\rangle$. The detunings $\delta_{\rm p}$ and $\delta_{\rm c}$ are chosen so that the spontaneous scattering rate in $|2\rangle$ is small enough to have long coherence times in $|2\rangle$, i.e., on the order of one second or more.

Striking differences between the cases of attractive (red detuned) and repulsive (blue detuned) disorder were observed and interpreted. The method of [20] is, however, strongly limited by a serious problem. It relies on a laser tuned *between* the two resonances associated with the two atomic ground levels, and the detuning for the upper state $|2\rangle$ cannot be large enough to avoid resonant scattering of photons in that state. This entails a rapid destruction of the coherence of the spatial wave function describing the atomic motion and thus of Anderson localization.

The method reported in the present paper overcomes this problem by the use of a bichromatic speckle potential. It consists of two speckles due to lasers of almost identical frequencies for which the potentials are of opposite signs for the initial state of the rf transfer, and of same signs for the final state of the rf transfer (Fig. 3). It yields a strong suppression of the sensitivity to the disorder in the initial state, together with a strong suppression of resonant scattering in the final—disorder sensitive—state. This scheme will allow one to operate with observation times around one second or more, which is required to study 3D localization phenomena [7,8].

This manuscript is organized as follows. In Sect. 2, we recall the most important properties of the state-dependent disordered potential based on a monochromatic laser speckle as used in Volchkov *et al.* [20] and discuss the limitations of that scheme. In Sect. 3, we describe the new method where we introduce a second laser to realize a bichromatic speckle. Firstly, we study the influence of the small difference between the two laser frequencies creating the two speckles and estimate the fundamental potential decorrelation in the disorder sensitive state, an important result of this paper. Secondly, we show how it is possible, by a suitable adjustment of the frequencies and intensities of the two lasers, to minimize the photon scattering rate in the disorder-sensitive state and to suppress the disorder experienced by the atoms in the initial state. In Sect. 4, we present an experimental evaluation of the bichromatic speckle disorder scheme. The reported measurements support our analysis and are promising for future quantum transport experiments.

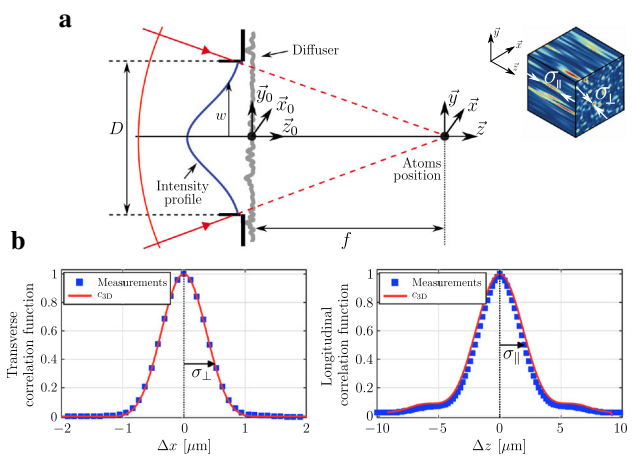

Fig. 4 **a** Sketch of the generation of the speckle in an effective paraxial geometry. A laser beam of waist w is focused using a lens of focal length $f = 15.2(5)$mm. A rough plate of diameter D scatters the laser light within an angle $\theta_{\text{diff}} \approx 5°$ which is fixed by the diffuser. The atomic cloud is centered on the optical axis in the Fourier plane $\{x = 0, y = 0, z = 0\}$. Inset: 3D view of a numerical realization of a speckle pattern. We define the size of the speckle grains by the half-widths $\sigma_\perp$ and $\sigma_\parallel$ of its autocorrelation function. **b** Measured transverse $c_{3D}(\Delta\mathbf{r}_\perp, \Delta z = 0)$ and longitudinal $c_{3D}(\Delta\mathbf{r}_\perp = \mathbf{0}, \Delta z)$ autocorrelation functions of the speckle pattern, fitted by an effective paraxial theoretical model with effective parameters $D = 17.8(1)$mm and $w = 8(1)$mm [36] (see text). This effective paraxial model successfully reproduces the features of the measured correlation functions.

2 State-dependent disordered potential based on a monochromatic speckle

The creation of state-dependent potential for alkali atoms has been widely investigated in the context of optical lattices using circularly polarized light tuned between the D_1 and D_2 lines, see, e.g., [32–34]. However, such scheme is efficient only if the two considered states have different magnetic susceptibilities [35]. Since the study of 3D Anderson localization requires a magnetic levitation to suspend the atoms against gravity during their expansion in the disorder [6–8], both disorder-sensitive and disorder-insensitive states must have similar magnetic susceptibility. Alternative methods to create state-dependent disorder must then be developed, such as the monochromatic speckle state-dependent potential realized in Ref. [20]. This section recalls the main properties of that scheme and points out its limits.

2.1 Monochromatic speckle potential

We consider the disordered potential $V(\mathbf{r})$ experienced by an atom in a specific level in the presence of a monochromatic laser speckle pattern of intensity $I(\mathbf{r})$. For a non-saturating laser strongly detuned from the nearest relevant resonance, it scales as $I(\mathbf{r})/\delta$, where $\delta = \omega - \omega_0$ is the detuning of the laser with respect to the nearest resonant transition involving the considered atomic level. The speckle is generated by focusing an expanded laser beam onto the atoms located in the focal plane and diffracting it through a rough plate of random thickness, as illustrated in Fig. 4. The simplest model of such a speckle, as presented in [37], results from the hypothesis that the rough plate imposes onto the laser beam a random phase $\phi(\mathbf{r}_0)$ with a probability distribution constant over 2π, and δ-correlated—meaning that the spatial autocorrelation function of the transmission $t_{\text{diff}}(\mathbf{r}_0) = \exp\{i\phi(\mathbf{r}_0)\}$ is a δ Dirac function.

The complex amplitude $\mathcal{A}(\mathbf{r})$ of the field at each point of the fully developed speckle pattern—close to the focus of the laser—can then be considered a sum of a very large number of independent random variables with the same statistical properties. According to the central limit theorem, the complex amplitude is thus a Gaussian random process, whose properties allow one to calculate the statistical properties of the intensity $I(\mathbf{r})$, which is proportional to the squared modulus $|\mathcal{A}(\mathbf{r})|^2$ of the complex amplitude. Since the complex amplitude at each point has a two-dimensional Gaussian probability distribution, the intensity $I(\mathbf{r})$ has an exponential probability distribution $\mathcal{P}(I) = \overline{I}^{-1} \exp[-I/\overline{I}]\Theta(I/\overline{I})$ [37] with Θ the unit step function, and where the symbol $\overline{\cdots}$ stands for ensemble averaging, i.e., averaging over different realizations of the rough plate. The standard deviation of the intensity fluctuations is then equal to the mean intensity value, i.e., $\sigma_I = \overline{I}$. A similar property $\sigma_V = |\overline{V}|$ holds for the disordered potential which can be positive or negative. It is experimentally controlled by adjusting the laser power and detuning and can be varied over several orders of magnitude [20]. Both $\overline{I}$ and $\overline{V}$ are independent of $\mathbf{r}$ because the process is spatially invariant and ergodic for this simple model of uncorrelated dephasing.

A key property of the fully developed speckle pattern is the size of the speckle grains, which is equal, within a factor, to the half-width of the normalized autocorrelation function defined around the focal point where the atoms are located

$$c_{3D}(\Delta\mathbf{r}_\perp, \Delta z) = \frac{\overline{\delta I(\mathbf{0}, 0)\, \delta I(\Delta\mathbf{r}_\perp, \Delta z)}}{\overline{\delta I^2}} \qquad (1)$$

Here, $\delta I(\mathbf{r}) = I(\mathbf{r}) - \overline{I}$ are the intensity fluctuations, and we note $\Delta\mathbf{r}_\perp = \{\Delta x, \Delta y\}$ the transverse displacement in the Fourier plane. The function c_{3D} is a fourth-order moment of the complex amplitude $\mathcal{A}(\mathbf{r})$, and for the Gaussian process considered here, one can use the Wick's theorem for classical moments of a Gaussian random process, to express any moment of $I(\mathbf{r})$ as a function of the second-order moments of the amplitude [37]. The function c_{3D} can then be expressed as a function of the autocorrelation function of the complex amplitude $\Gamma_{\mathcal{A}}(\Delta\mathbf{r}_\perp, \Delta z)$ (calculated in Sect. 1 of Appendix A) as

$$c_{3D}(\Delta\mathbf{r}_\perp,\Delta z)=\frac{|\Gamma_{\mathcal{A}}(\Delta\mathbf{r}_\perp,\Delta z)|^2}{|\Gamma_{\mathcal{A}}(\mathbf{0},0)|^2}=\frac{\left|\mathrm{FT}\left[I(\mathbf{r}_0)e^{-i\frac{\mathbf{r}_0^2 k\Delta z}{2f^2}}\right]_{\frac{k\Delta\mathbf{r}_\perp}{f}}\right|^2}{\left|\int \mathrm{d}\mathbf{r}_0\, I(\mathbf{r}_0)\right|^2} \quad (2)$$

This correlation function is central to quantum transport studies as it directly translates into the spatial frequency distribution of the potential that governs the scattering properties of the atoms [9,36,38–40]. A full calculation is presented in section A.3 of Appendix A, and here, we only discuss some of its most important features in the transverse and longitudinal directions.

Within the paraxial approximation, the transverse amplitude correlation function $\Gamma_{\mathcal{A}}(\Delta\mathbf{r}_\perp,\Delta z=0)$ is the Fourier transform of the intensity distribution $I(\mathbf{r}_0)$ just before the diffusing plate [37]. This can be interpreted as an example of the Van Cittert-Zernike theorem [41]. The intensity fluctuations correlation function is thus nothing else than the squared modulus of the diffraction pattern corresponding to the intensity distribution at the diffusing plate in the diffuser

$$c_{3D}(\Delta\mathbf{r}_\perp,\Delta z=0)\propto\left|\mathrm{FT}\left[I(\mathbf{r}_0)\right]_{\frac{k\Delta\mathbf{r}_\perp}{f}}\right|^2. \quad (3)$$

For instance, in the ideal case of a Gaussian intensity profile of standard waist radius w (following the usual convention for laser beams, w is the radius at e^{-2}), it is

$$c_{3D}(\Delta\mathbf{r}_\perp,\Delta z=0)=\exp\left\{-\frac{\Delta\mathbf{r}_\perp^2}{\sigma_\perp^2}\right\}, \quad (4)$$

with $\sigma_\perp=\lambda f/\pi w$. We call $\sigma_\perp$ the size of a speckle grain, for consistency with previous papers. Within the same paraxial hypothesis, the longitudinal autocorrelation function of the intensity fluctuations is, on the z axis and close to the focusing point of the lens [37]

$$c_{3D}(\mathbf{0},\Delta z)\propto\left|\int \mathrm{d}\mathbf{r}_0 I(\mathbf{r}_0)\exp\left\{-ik\frac{\mathbf{r}_0^2\Delta z}{2f^2}\right\}\right|^2. \quad (5)$$

In general, the evaluation of the integral in (5) can be done numerically only. In the ideal case of a Gaussian intensity profile, it yields a Lorentzian profile of the longitudinal correlation function [37] and we define the size of a speckle grain by the half-width at half-maximum $\sigma_\parallel$.

A more realistic description of the situation[37] considers a correlated diffuser with a spatial autocorrelation function of the phase factor—more precisely of $\exp\{i\phi(\mathbf{r}_0)\}$—of finite width r_e (see section A.1 of the appendix). The speckle pattern has then a mean intensity profile that is no longer uniform, in contrast to the δ-correlated model above. This profile is given by the Fourier transform of the autocorrelation function of the phase factor. For our diffuser, it has a Gaussian shape with an angular width of about $\theta_\mathrm{diff}\approx 5°$ ($1/e^2$ radius) and yields a speckle pattern extending on a zone much wider ($\sim 1.3\,\mathrm{mm}$) than the atomic cloud ($\sim 15\,\mu\mathrm{m}$). The average intensity on the atoms is then almost constant and the speckle can still be considered uniform over the atoms sample. Moreover, the correlation length of the phase factor of the rough plate is small compared to the width w of the laser beam on the plate, so that the central limit theorem still applies to the speckle complex amplitude which is well represented by a Gaussian statistics. We can thus use the formulae (3) and (5).

Another more realistic feature of our experiment is the fact that the phase distribution at the diffuser may not be strictly uniform over 2π. In fact, as shown in [42] and in section A.1 of the Appendix A, a model with a Gaussian phase distribution of standard deviation σ_ϕ allows us to show that the formulae (3) and (5) can still be used as long as $\sigma_\phi\gg 2\pi$, for a monochromatic speckle. We will see in Sect. 3 that a bichromatic speckle requires a more elaborated description, for which we will use the model of a plate with a Gaussian distribution of thickness.

The experimental determination of the correlation function (1) was done with an optical microscope [43] and the results are shown in Fig. 4b. Because of the large numerical aperture $\mathrm{NA}=0.55(2)$, the theoretical description requires a beyond-paraxial model [20]. In fact, the measured transverse and longitudinal correlation functions were found well reproduced by equations (3) and (5), provided that we introduce a geometrical scaling factor [36,44]. More precisely, we can match the measured correlation functions using formulae (3) and (5) with a geometrical factor of 0.875, resulting in the effective numerical aperture $\mathrm{NA}_\mathrm{eff}=0.50$. In particular, the transverse profile of the three-dimensional correlation function is very well described by a Gaussian function (4) of $1/e$ radius $\sigma_\perp=0.50(1)\mu\mathrm{m}$. The longitudinal profile is also well reproduced by the result of a numerical evaluation of (5) based on a truncated Gaussian illumination[1] [36]. A longitudinal correlation length can still be defined by the half-width at half-maximum, yielding $\sigma_\parallel=2.05(5)\,\mu\mathrm{m}$ [20]. Altogether, this indicates that an effective paraxial approximation is well suited to describe the spatial correlations of our speckle.

2.2 Energy-resolved transfer scheme in a monochromatic state-dependent optical potential for ^{87}Rb

In this subsection, we address the two problems that influence the energy spread of ^{87}Rb atoms transferred

[1] The case of a pure Gaussian intensity profile on the diffuser leads to a Lorentzian longitudinal correlation function, while it is described by a sinc^2 function in the case of a circularly truncated homogeneous illumination. In both cases, we characterize its width by the HWHM.

into a disordered potential: the fluctuations of the energy difference between the magnetic levels due to magnetic field fluctuations, and the energy dispersion of the initial state.

2.2.1 Suppression of the effect of the magnetic field fluctuations

The atomic sample consists of a Bose-Einstein Condensate (BEC) prepared in the disorder-insensitive state $|1\rangle$ with energy E_1 and then coupled by a rf field to the disorder sensitive state $|2\rangle$ with energy E_2. The final kinetic energy E_f relevant to the transport is $E_f = E_i + \hbar\delta_{\rm rf}$ where E_i is the initial kinetic energy, which is null for atoms initially at rest, and $\delta_{\rm rf} = \omega_{\rm rf} - \Delta_{\rm hf}$ is the detuning of the rf field with respect to the bare $|1\rangle \rightarrow |2\rangle$ transition. The energy E_f can be chosen by tuning the rf frequency, allowing us to address precise energy values of the atoms in the disorder-sensitive state.

If the bare resonance frequency $\Delta_{\rm hf}$ between the two magnetic sublevels fluctuates because of magnetic field fluctuations, the energy E_f will also fluctuate. In order to cancel these fluctuations of E_f, we use the so-called clock states $|1\rangle \equiv |F = 1, m_{\rm F} = -1\rangle$ and $|2\rangle \equiv |F = 2, m_{\rm F} = +1\rangle$, which are separated at zero field by a splitting of $\Delta_{\rm hf}/2\pi = 6.835\,{\rm GHz}$, and we impose a bias magnetic field at the so-called *magic* value of $B_0^* = 3.23\,{\rm G}$. The magnetic susceptibilities of states $|1\rangle$ and $|2\rangle$ of ^{87}Rb are then identical, meaning that the energy separation between these states is insensitive to magnetic field fluctuations [45]. Moreover, this choice of the clock states is also crucial regarding the use of the magnetic levitation to study the propagation of the atoms in 3D.

The rf coupling consists in fact of a two-photon transition, involving a microwave and a rf field, to match the angular momentum difference $\Delta m_F = 2$ [20]. It can be considered as a direct transition induced by a field with an effective frequency $\omega_{\rm rf}$ equal to the sum of the two frequencies of the two fields, and an effective Rabi frequency proportional to the product of the Rabi frequencies of the two fields.

2.2.2 Suppression of the sensitivity of the initial state to the disordered potential

In order to have a speckle acting strongly on the atomic state $|2\rangle$ but very little on the atomic state $|1\rangle$, we use a laser of frequency ω close to resonance for the transition $|2\rangle \rightarrow |F'\rangle$ and far from resonance for the transition $|1\rangle \rightarrow |F'\rangle$ (see Fig. 2). More precisely, since the natural linewidth of the transition ($\Gamma_{\rm Rb}/2\pi \simeq 6.07\,{\rm MHz}$) is small compared to the splitting $\Delta_{\rm hf}/2\pi \simeq 6.8\,{\rm GHz}$ [46], it is possible to operate in the regime of $\Gamma_{\rm Rb} \ll \delta \ll \Delta_{\rm hf}$, with $\delta = \omega - \omega_{2,F'}$ the detuning of the speckle laser from resonance for state $|2\rangle$. Then, the detuning from resonance for state $|1\rangle$ is almost equal to $\Delta_{\rm hf}$, so that the average speckle potentials for level $|1\rangle$ and level $|2\rangle$ are in a ratio

$$\frac{V_1}{V_2} \sim \frac{\delta}{\Delta_{\rm hf}} \ll 1\,. \tag{6}$$

With well-chosen laser intensity I and detuning δ, one can then obtain an almost disorder-insensitive state $|1\rangle$, i.e., a disordered potential V_1 small compared to the chemical potential μ, so that the screening effect in the Bose-Einstein condensate prepared in state $|1\rangle$ absorbs the residual potential V_1 and suppresses further its eventual perturbation [47]. In contrast, state $|2\rangle$ is sensitive to the disorder, as expected. For instance, the choice of $\delta/2\pi \approx \pm 80\,{\rm MHz}$ in Volchkov et al. leads to a disordered potential ratio of $|V_2/V_1| \sim 100$ with $V_1 \leq \mu$.

This simple implementation of a state-dependent disordered potential allowed us to determine the spectral functions of ultracold atoms in a speckle potential at various energies. The results were found in remarkable agreement with a numerical theoretical treatment in all regimes of disorder [20]. This result shows the interest of a transfer between a weakly disorder-sensitive state and a strongly disorder-sensitive state, in order to make energy-resolved measurements on transport of atoms in disorder.

However, equation (6) with the requirement $V_1 < \mu$ prevents one to have a large value of δ, so that the spontaneous photon scattering rate in state $|2\rangle$, which scales as $\Gamma \sim I/\delta^2$, is large enough to make it impossible to study quantum transport of the atoms in state $|2\rangle$ for a long time. This is because the spontaneous scattering of a photon by an atom in state $|2\rangle$ destroys the motional wave function coherence, which is at the heart of quantum transport and Anderson localization. For instance, in the configuration of Volchkov et al., the photon scattering rate was as large as a few $10^3\,{\rm s}^{-1}$, forbidding measurement times beyond a few milliseconds, see Table 1. This inadequacy of the monochromatic speckle potential to allow for long-lasting energy-resolved quantum transport experiments can be overcome by the use of a bichromatic speckle potential, as explained in next section.

3 State-dependent disordered potential based on a bichromatic speckle

In Sect. 3.1, we present the improved scheme to experimentally study quantum transport of atoms, based on a disordered potential created by two lasers at two different frequencies. In Sect. 3.2, we give a quantitative evaluation of the residual disorder due to a fundamental potential decorrelation resulting from the difference in frequencies between the two lasers. It is characterized by a normalized bichromatic correlation function, whose form is remarkable. It allows us to show that the residual disorder in state $|1\rangle$ has the same order of magnitude as in the monochromatic scheme. In Sect. 3.3, we evaluate the residual spontaneous scattering rate of laser photons in state $|2\rangle$, and we show that is reduced

by several orders of magnitude, which is the main goal of the new scheme.

3.1 Bichromatic speckle scheme

As shown in Fig. 3, we use two lasers sufficiently detuned from resonance with state $|2\rangle$. The principal laser (purple in Fig. 3) is largely detuned and we fix its detuning $\delta_\mathrm{p}/2\pi = 95\,\mathrm{GHz}$ with respect to the transition $|1\rangle \rightarrow |F'\rangle$. The potential on state $|1\rangle$ is suppressed by the use of a less-detuned compensation laser (orange in Fig. 3), with an opposite detuning sign. We can add the two potentials without considering possible interferences between the lasers because the beat-note frequency ($\sim 100\,\mathrm{GHz}$ in the implementations presented below) is high enough that it is averaged out by the inertia of the atoms and has no effect on the atomic motion. In the linear regime, the total disordered potential for atoms in state $|F, m_F\rangle$ can thus be written as

$$V_{F,m_F}(\mathbf{r}) = -\frac{1}{2\epsilon_0 c}\big(\,\mathrm{Re}[\alpha_{F,m_F}(\delta_\mathrm{p})]I_\mathrm{p}(\mathbf{r}) + \mathrm{Re}[\alpha_{F,m_F}(\delta_\mathrm{c})]I_\mathrm{c}(\mathbf{r})\,\big)\,, \tag{7}$$

where the complex atomic polarizability $\alpha_{F,m_F}(\delta)$ describes the atomic dipolar response of the internal state $|F, m_F\rangle$ to an external electric field of detuning $\delta = \omega - \omega_{1,F'}$. The subscript p stands for principal and c stands for compensation.

Following the scheme sketched in Fig. 3, we want to adjust the two potentials such that they cancel each other in state $|1\rangle$, while summing up in state $|2\rangle$. We denote V_R the amplitude of the total laser speckle field in this disorder-sensitive state, which is the relevant quantity when considering the study of quantum transport phenomena in such disordered potential. These two conditions write

$$\begin{cases} V_1(\mathbf{r}) = V_{\mathrm{p},1}(\mathbf{r}) + V_{\mathrm{c},1}(\mathbf{r}) \\ V_2(\mathbf{r}) = V_{\mathrm{p},2}(\mathbf{r}) + V_{\mathrm{c},2}(\mathbf{r}) \end{cases} \text{with} \begin{cases} \overline{V_1} = 0 \\ \overline{V_2} = V_\mathrm{R} \end{cases} \tag{8}$$

Canceling the total potential $V_1(\mathbf{r})$ on state $|1\rangle$ for all $\{\mathbf{r}\}$ requires the two speckle patterns to be as identical as possible. To do so, a first mandatory condition is to shine two identical laser modes on the diffuser (as shown in Fig. 4 for a single laser beam). This is experimentally done by injecting the two lasers into the same optical fiber before shining them onto the diffuser.

A second condition lies in the stability of the laser intensities. Power fluctuations of one of the beams of the order of a few percent can lead to strong potential fluctuations on state $|1\rangle$—up to a few percent of V_R—which can be limiting, see Table 1. Each of the lasers are therefore power-stabilized.

However, strict equality of the two identical speckle patterns cannot be achieved with different wavelengths, because the speckle patterns depend on diffraction and therefore on the laser wavelengths. The use of different laser wavelengths then leads to fundamental potential decorrelation preventing the complete canceling of the disorder for state $|1\rangle$. That is the subject of the next section.

3.2 Fundamental potential decorrelation in the disorder-insensitive state

Recalling that the detunings and intensities of the two lasers are adjusted such that $\overline{V_{\mathrm{c},1}} = -\overline{V_{\mathrm{p},1}}$, we want to characterize the residual fluctuations $\delta V_1(\mathbf{r}) = \delta V_{\mathrm{p},1}(\mathbf{r}) + \delta V_{\mathrm{c},1}(\mathbf{r})$ due to the frequency difference between the two lasers. We thus evaluate the variance of $V_1(\mathbf{r})$ at each point. For a speckle pattern, one has $\sigma_V = \overline{V}$, and the variance can be expressed as

$$\sigma^2_{V_1}(\mathbf{r}) = 2|\overline{V_{\mathrm{p},1}}(\mathbf{r})\,\overline{V_{\mathrm{c},1}}(\mathbf{r})|\,(1 - c_{2\lambda}(\mathbf{r}, \lambda_\mathrm{p}, \lambda_\mathrm{c}))\,, \tag{9}$$

where the normalized bichromatic correlation function $c_{2\lambda}$ is defined as

$$c_{2\lambda}(\mathbf{r}, \lambda_\mathrm{p}, \lambda_\mathrm{c}) \equiv \frac{\overline{\delta V_{\mathrm{p},1}(\mathbf{r})\delta V_{\mathrm{c},1}(\mathbf{r})}}{\overline{V_{\mathrm{p},1}(\mathbf{r})}\,\overline{V_{\mathrm{c},1}(\mathbf{r})}}\,. \tag{10}$$

The correlation function (10) quantifies the correlation of the two speckle fields at position $\mathbf{r}$ in space as a function of their wavelengths. In the case of totally decorrelated speckle fields ($c_{2\lambda} = 0$), the variance of the total potential is consistently given by the sum of the variances of each field. In contrast, for exactly identical speckle patterns, the variance of the total potential would be null. Studying the amplitude of the residual potential then comes down to investigating the behavior of the normalized bichromatic correlation function $c_{2\lambda}(\mathbf{r}, \lambda_\mathrm{p}, \lambda_\mathrm{c})$.

Relying on the same paraxial assumption as for the calculation of the spatial correlation function of a single speckle pattern, we find (see Appendix A) that the correlation function between the two speckles generated by the same diffuser, for the same spatial mode but for different frequencies, can be expressed as

$$c_{2\lambda}(\mathbf{r}_\perp, z, \lambda_\mathrm{p}, \lambda_\mathrm{c}) = e^{-\sigma^2_{\Delta\phi}}\, c_{3D}\Big(\frac{\mathbf{r}_\perp}{\mathcal{F}}, \frac{z}{\mathcal{F}}\Big)\,, \tag{11}$$

where $\sigma_{\Delta\phi}$ is a term discussed below and the parameter $\mathcal{F} = \omega_\mathrm{p}/\delta\omega = \lambda_\mathrm{p}/\delta\lambda \approx 4000$ characterizes the frequency difference of the two speckle fields. Expression (11) constitutes a major result of this letter. It is the product of two terms that have a simple interpretation.

The first term $\exp\{-\sigma^2_{\Delta\phi}\}$ is associated to the fluctuations of the phase difference for the two different wavelengths λ_p and λ_c propagating inside the rough plate at the same point. More precisely, the phases at each point of the diffuser differ for the two lasers according to $\Delta\phi(\mathbf{r}_0) = \phi_\mathrm{p} - \phi_\mathrm{c} = 2\pi(n-1)(\lambda_\mathrm{p}^{-1} - \lambda_\mathrm{c}^{-1})\delta e(\mathbf{r}_0)$, where δe corresponds to the thickness fluctuations. When averaged over the diffuser, i.e., over $\mathbf{r}_0$, and considering a Gaussian distribution for the phase as discussed in Sect. 2.1, one obtains an average phase factor $\overline{\exp\{i\Delta\phi\}} = \exp\{-\sigma^2_{\Delta\phi}/2\}$, with $\sigma^2_{\Delta\phi}$ the variance of $\Delta\phi$. This fluctuating phase difference term

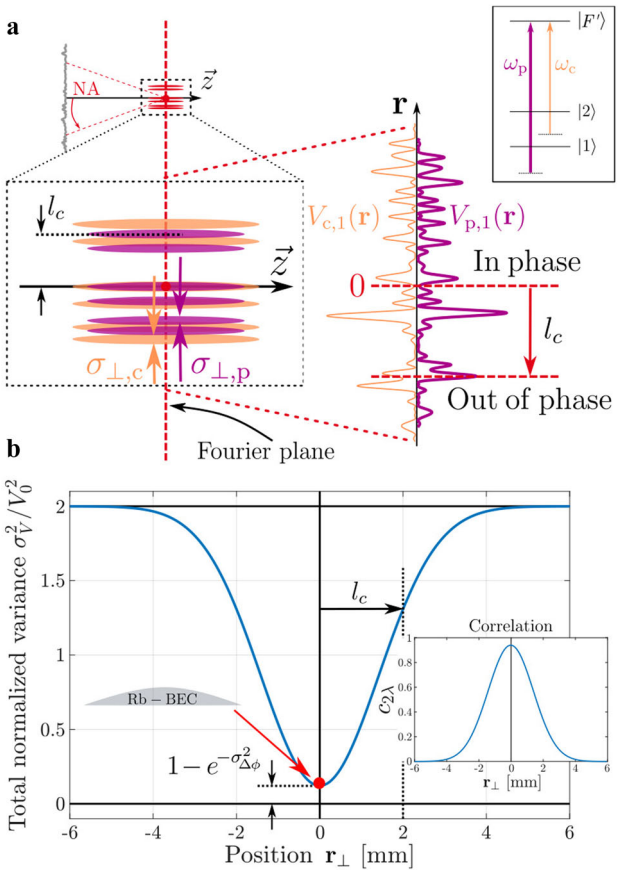

Fig. 5 **a** Illustration of the correlation between two speckle potentials generated by the same diffuser with two slightly different wavelengths. Close to the Fourier plane, the two patterns are identical up to a spatial scaling factor, yielding an almost perfect overlap of the potential that decreases with the distance to the optical axis. The correlation length l_c describes the typical distance for which the speckle patterns become out of phase. **b** Plot of the variance of the total potential as a function of the position in the Fourier plane. Close to the optical axis, the two speckle patterns are similar and the only decorrelation term arises from the phase difference due to the propagation through the diffuser. Far away from the optical axis, the two speckle patterns do not superimpose and the variance of the total potential is the sum of the two individual variances. Plot obtained for a realistic inverse relative frequency difference $\mathcal{F} = 4000$, a well-exaggerated diffuser's roughness $\sigma_e^2 = 10^5\lambda_p^2$ and potentials of opposite average values V_0.

therefore results into a decorrelation factor constant in the speckle pattern. It is solely due to the roughness of the diffusing plate, and it can be rewritten as $\exp\{-\sigma^2_{\Delta\phi}\} \approx \exp\{-4\pi^2(n-1)^2\sigma_e^2/\lambda_p^2\mathcal{F}^2\}$[2]. Here, σ_e is the thickness fluctuations r.m.s. value, i.e., the diffuser's roughness. It means that the rougher the diffuser and the bigger the frequency difference, the less the speckle patterns will be correlated, even at the center of the patterns. This term has been visually exaggerated in Fig. 5b and explains why the minimum of the variance does not reach perfectly 0.

In practice, the diffuser's roughness σ_e is fixed by manufacturing. It was measured at the optics workshop of Institut d'Optique, using a profilometer. Several measurements of the surface's profile have been performed along 1 mm long straight lines onto several areas of our diffuser, leading to a r.m.s. roughness of $\sigma_e = 1.3\,\mu$m. For $\mathcal{F} \approx 4000$, the term $e^{-\sigma^2_{\Delta\phi}}$ (associated to the first factor of expression 11) is $\sim 1-10^{-6}$, indicating almost perfect correlation between the two speckles and thus a negligible residual disorder.

The second contribution in equation (11) describes the loss of correlation as the position in the speckle is shifted away from the optical axis. It is due to the different geometrical scaling factors of the two speckle patterns, proportional to the wavelengths, as illustrated in Fig. 5. Remarkably, the resulting term is expressed with the spatial correlation function (1) of a monochromatic speckle, with a magnifying factor $\mathcal{F}$. The bichromatic correlation function then has a width $l_c = \mathcal{F}\sigma_\perp$ which defines a "bichromatic correlation length," corresponding to the distance from the center at which the two patterns are shifted by one speckle grain size.

This correlation length must be compared to the maximum size of the atomic sample. Taking again $\mathcal{F} \approx 4000$ corresponding to a frequency difference $\delta\omega/2\pi \approx 100$ GHz (see Sect. 3.1), the bichromatic correlation length is of the order of $l_c \sim 2$ mm. It is much larger than the largest size of our atomic sample about $R_{TF} \sim 45\,\mu$m, see Sect. 4. We can then estimate this decorrelation factor to be at most $1 - c_{3D}(R_{TF}/\mathcal{F}) \sim 5\times10^{-4}$. Altogether, we find using Eq. (9) that the fundamental potential decorrelation leads typically to a residual disorder in state $|1\rangle$ with a r.m.s. value of the order of

$$\sigma_{V_1} \sim 0.02 \times V_R\,, \tag{12}$$

i.e., of the same order as in Volchkov *et al.* [20], see discussion in 2.2.2. For instance, we will see below that Table 1 predicts a residual disorder $\sigma_{V_1}/h = 11.4$ Hz for the specific case of $V_R/h = 416$ Hz, in agreement with the coarse estimation of expression (12).

3.3 Reduction in the photon scattering rate for the disorder-sensitive state

Let us recall that a strong reduction in Γ_2, the photon scattering rate of the disorder-sensitive state $|2\rangle$, is the main goal of our present work. In order to study quantum transport phenomena such as Anderson localization, a lifetime on the order of one second time or more is needed [7,8]. Note that, the condition is much less stringent in the initial state, being only on the order of tens of milliseconds. This state $|1\rangle$ is indeed only used as a "source" of atoms of very well-defined energy

[2] The factor two compared to the first factor in Eq. (11) is due to the fact that we consider the correlation of the potential that is proportional to the light intensity and not to the field amplitude, see appendix A.

Table 1 Comparison of the state-dependent disordered potential parameter between the monochromatic configuration and the bichromatic one, the crucial quantity being the photon scattering lifetime in state $|2\rangle$ (Γ_2^{-1}, bolded line).

Quantity	Monochromatic case	Bichromatic case
$\delta/2\pi$	81 MHz	—
$\delta_\mathrm{p}/2\pi$	—	95 GHz
$\delta_\mathrm{c}/2\pi$	—	−1.40 GHz
Γ_1^{-1}	26.6 s	73 ms
$\mathbf{\Gamma_2^{-1}}$	**5.3 ms**	**1.66 s**
σ_{V_1}/h	6.3 Hz	11.4 Hz
P	0.49 μW	—
P_p	—	430 μW
P_c	—	4.6 μW

The determination of these quantities has been performed for a total disorder amplitude of $V_\mathrm{R}/h = 416$ Hz. The quantities δ_p and δ_c are defined in Fig. 3 and δ is defined in Fig. 2. P, P_p, and P_c correspond to the laser powers.

during the rf transfer[3], yielding the simpler condition $\Gamma_1^{-1} \geq t_\mathrm{rf}$ (see Sect. 2.2).

In presence of the bichromatic potential, the total photon scattering rate is given by the sum of the individual rates, proportional to the imaginary parts of the atomic polarizability, in the linear regime:

$$\Gamma_{F,m_F} = \frac{1}{\hbar\epsilon_0 c}\Big(\mathrm{Im}[\alpha_{F,m_F}(\delta_\mathrm{P})]I_\mathrm{p} + \mathrm{Im}[\alpha_{F,m_F}(\delta_\mathrm{c})]I_\mathrm{c}\Big). \quad (13)$$

Table 1 shows the results of the numerical determination of the experimental parameters for a bichromatic speckle potential corresponding to $V_\mathrm{R}/h = 416$ Hz. This value is typical for the experimental study of the Anderson localization or the spectral functions (see Refs. [7,20]). For consistency, this value will also correspond to the experiments described in the next section.

Here, the detuning of the principal laser is set to $\delta_\mathrm{p}/2\pi = 95$ GHz. This value is chosen as a compromise to get a sufficiently large detuning, while the two speckle patterns can be considered identical enough to permit the cancelation of the total potential onto the disorder insensitive state. Then, the detuning δ_c of the compensation laser is determined so that the lifetime of state $|1\rangle$ is larger than the duration of rf transfer (for instance $t_\mathrm{rf} = 40$ ms for the experiment shown in Sect. 4). Here, we have $\delta_\mathrm{c}/2\pi = -1.40$ GHz and $\Gamma_1^{-1} = 73$ ms. With these parameters, one can in particular deduce the potential amplitude generated by both the laser speckle fields on the state $|1\rangle$ and $|2\rangle$: $V_{\mathrm{p},1}/h = -V_{\mathrm{c},1}/h = 366$ Hz, $V_{\mathrm{p},2}/h = 348$ Hz and $V_{\mathrm{c},2}/h = 68$ Hz.

[3] Once the rf transfer is switched off, the atoms in the state $|1\rangle$ can be removed to avoid any detrimental interactions with the atoms transferred in the state $|2\rangle$.

The most notable result of Table 1 is the improvement of the scattering lifetime Γ_2^{-1} of the disorder-sensitive state $|2\rangle$ by more than two orders of magnitude, going from a few milliseconds for the monochromatic configuration of [20] up to more than one second in the bichromatic configuration. Additionally, the residual disordered potential σ_{V_1} applied to the disorder-insensitive state is of the same order as in the monochromatic configuration, yielding the same state-selectivity.

The analysis described here for the specific case of $V_\mathrm{R}/h = 416$ Hz can be reproduced for a wide range of disorder amplitudes, both for a globally attractive ($V_\mathrm{R} < 0$) and repulsive ($V_\mathrm{R} > 0$) disorder in state $|2\rangle$, leading to the same conclusion. For instance, we checked that we obtain similar improvements for the range of disorder amplitudes $|V_\mathrm{R}/h| \in [40\,\mathrm{Hz}, 4\,\mathrm{KHz}]$ used in Volchkov et al. [20].

4 Experimental check of the bichromatic speckle configuration

In this section, we present an evaluation of the new bichromatic disordered potential scheme with ultracold atoms. More precisely, we focus on two main aspects. Firstly, we check the efficient subtraction of the two speckle potentials in the state $|1\rangle$, as described in Fig. 3, so that it is merely insensitive to the disordered potential. This is done by studying the mechanical excitation of the atoms in state $|1\rangle$ following a quench of the disorder potential. Secondly, we realize the rf transfer protocol as demonstrated in Volchkov et al. [20] (see Fig. 1) and measure the spontaneous scattering lifetime of the atoms transferred in state $|2\rangle$. As predicted in Table 1, we find a large improvement by two orders of magnitude compared to the monochromatic speckle case, the lifetime being now on the second time scale.

4.1 Experimental setup

The starting point of the experiment is the creation of a BEC of ^{87}Rb atoms in the hyperfine state $|1\rangle \equiv |F = 1, m_F = -1\rangle$. The atoms are confined in a crossed optical dipole trap, formed by two orthogonal laser beams at a wavelength of 1070 nm, in presence of a magnetic levitation. As described in Ref. [48], the magnetic levitation is created by adding a magnetic gradient, whose force acts against gravity, to the magic bias field of 3.23 G (see Sect. 2.2.1).

The magnetic levitation enables us to end up the optical evaporation process with a very decompressed trap configuration ($\omega_y \simeq 5$ Hz, $\omega_z/2\pi \simeq 25$ Hz and $\omega_x/2\pi \simeq 30$ Hz). At this stage, we obtain a BEC with around 2×10^5 atoms, corresponding to a chemical potential around $\mu/h \simeq 250$ Hz and a Thomas-Fermi radii around $R_\mathrm{TF} \sim 45$, 10 and 8 μm along each direction. In the Thomas-Fermi regime, the meanfield interatomic interactions compensate perfectly the trapping

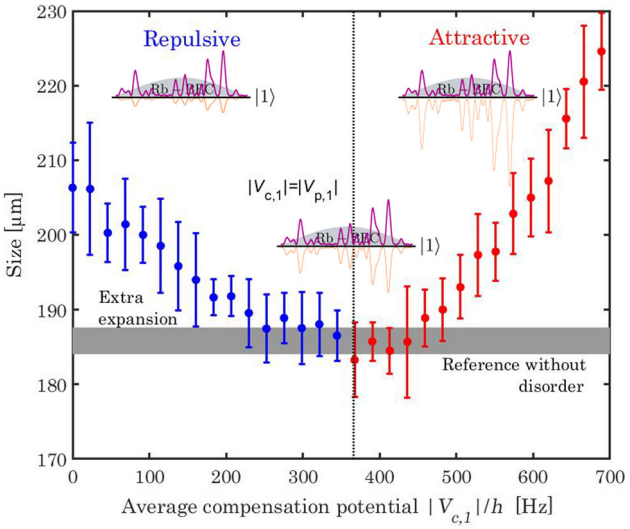

Fig. 6 Evolution of the momentum distribution of the atoms in state $|1\rangle$ following a sudden switch on of the bichromatic speckle potential (quench protocol). The amplitude of the principal potential amplitude is fixed to $V_{\mathrm{p},1}/h = 366$ Hz, while the amplitude of compensating potential is scanned from $|V_{\mathrm{c},1}|/h$=0 to 700 Hz. The dots correspond to the atomic cloud r.m.s. size measured by fluorescence imaging after a time of flight of 200 ms. The error bars correspond to the rms uncertainties estimated over five experimental realizations. For clarity, the dots are colored in blue when the total disorder amplitude $V_1 = V_{\mathrm{p},1} + V_{\mathrm{c},1}$ is repulsive and in red when it is attractive—see illustrations. The horizontal line corresponds to the reference case where no disorder is applied to the atoms. The vertical dotted line indicates the theoretical condition for an optimal cancelation of the total disorder potential in state $|1\rangle$, that is $|V_{\mathrm{c},1}| = V_{\mathrm{p},1}$.

potential [48], resulting in an overall flat potential for atoms in state $|1\rangle$ and in state $|2\rangle$ in the absence of the disordered potential, as sketched in Figs. 1, 2 and 3.

The laser speckle disorder geometry and parameters have been extensively detailed in Sects. 2.1 and 3. Let us note, however, that the precise disorder amplitude calibration is a well-known issue for experiments. As shown in [48], an efficient method relies on direct comparison between directly measured spectral functions and numerical calculations. The same method is thus applied here using the spectral function obtained for our reference disorder amplitude value $V_{\mathrm{R}}/h = 416$ Hz (see Sect. 4.3).

4.2 Probing the insensitivity of state $|1\rangle$ to disorder using a quench

In order to quantify the effect of the residual disorder in state $|1\rangle$, we introduce a quench protocol. To do so, we switch on abruptly the total disordered potential (within 100 μs) and keep it on for 4 ms. Then, the disorder is switched off and we measure the momentum distribution of the atoms in $|1\rangle$ using a standard time of flight technique of duration $t_{\mathrm{ToF}} = 200$ ms.

The evolution of the atomic momentum distribution is shown in Fig. 6, where we scan the amplitude of the compensation potential from $|V_{\mathrm{c},1}|/h = 0$ to 700 Hz ($V_{\mathrm{c},1}$ being attractive), while the principal potential is kept constant $V_{\mathrm{p},1}/h = 366$ Hz ($V_{\mathrm{p},1}$ being repulsive). These parameters are chosen to explore the typical configuration predicted in Table 1, where the state $|2\rangle$ experiences the total potential $V_{\mathrm{R}}/h = 416$ Hz while the disorder is ideally suppressed in state $|1\rangle$ for $V_{\mathrm{c},1} = -V_{\mathrm{p},1}$ (see Sect. 3.2).

For very low compensation amplitude, $|V_{\mathrm{c},1}| \ll V_{\mathrm{p},1}$, the total potential in state $|1\rangle$ is essentially given by the "principal" disorder potential. This repulsive potential excites the BEC when the disorder is switched on, a part of the potential energy being transfer to the kinetic energy. This extra kinetic energy results in a broadening of the atomic momentum distribution (see horizontal line corresponding to the absence of disorder as a reference).

As the compensating potential is increased, the total disordered potential in $|1\rangle$ decreases and the momentum distribution spread decreases accordingly, with a minimum at the best compensation. When $|V_{\mathrm{c},1}| > V_{\mathrm{p},1}$, the total potential V_1 turns to attractive, and the disorder strength increases again. The momentum distribution broadens then in this regime. The minimum is reached as expected around $|V_{\mathrm{c},1}| = V_{\mathrm{p},1}$ (vertical thin dotted line), and, most importantly, we observe a momentum spread exactly equal to the one in the absence of disorder. This observation is a strong evidence of the efficient compensation of the two disordered potentials, the residual potential yielding no observable excitation of the atomic cloud in $|1\rangle$.

4.3 Improved lifetime in the disorder-sensitive state $|2\rangle$

The expected suppression of the disordered potential in state $|1\rangle$ being verified, we perform the rf transfer toward the disorder-sensitive state $|2\rangle$ at the energy defined by $\delta_{\mathrm{rf}} = \omega_{\mathrm{rf}} - \Delta_{\mathrm{hf}}$ (see Fig. 1 and discussion in Sect. 2.2.1). Here, we continue to investigate the configuration of Table 1 and we set the bichromatic disorder parameters at the minimum point of Fig. 6, that is for $|V_{\mathrm{c},1}|/h = V_{\mathrm{p},1}/h = 366$ Hz. The rf power is chosen low enough to operate in the weak coupling regime where the transfer rate $\Gamma(\delta_{\mathrm{rf}})$ is well predicted by the Fermi Golden rule [48]. Moreover, the rf field is applied in the regime of $\Gamma t_{\mathrm{rf}} \ll 1$ (with $t_{\mathrm{rf}} = 40$ ms) so that only a small fraction of the atoms are transferred to state $|2\rangle$ (not more than 25% at most). As discussed in Sect. 3.3, note that, the rf duration is also chosen to be shorter than the lifetime in state $|1\rangle$. In these conditions, the energy resolution is time Fourier-limited to $\Delta E/h = 1/t_{\mathrm{rf}} = 25$ Hz.

Figure 7a shows the evolution of the transferred atom number as a function of the rf detuning δ_{rf}, for a fixed rf power. As explained in [20], the curve $\Gamma(\delta_{\mathrm{rf}})$ constitutes a direct measurement of the spectral function for the disordered potential in state $|2\rangle$. A comparison is shown

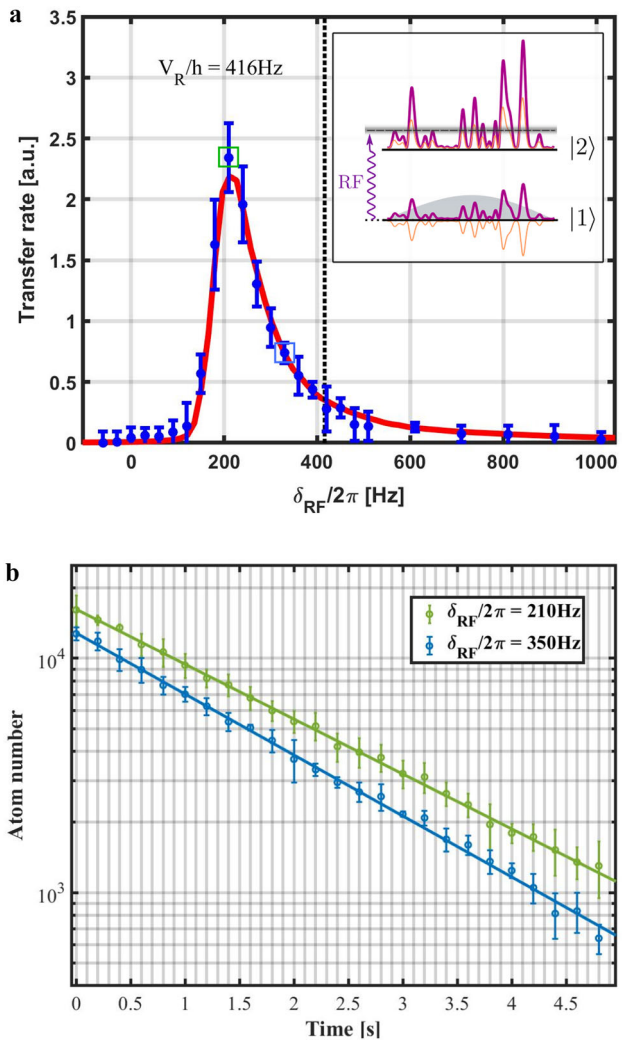

Fig. 7 Implementation of the rf transfer scheme and lifetime measurement for $V_R/h = 416$ Hz. a) Normalized transfer rate $\Gamma(\delta_{rf})$ from disorder insensitive state $|1\rangle$ to the disorder-sensitive state $|2\rangle$. The compensating and principal disorder amplitudes are set to $|V_{c,1}|/h = V_{p,1}/h = 366$ Hz, that is the optimal cancelation condition for the disorder in state $|1\rangle$ (see Fig. 6). The rf power is fixed and the rf field is applied during $t_{rf} = 40$ ms. The blue dots are the measured points and the red curve is the numerical calculation in [20], taking into account the resolution $\Delta E/h = 1/t_{rf} = 25$ Hz. The squares correspond to the detunings δ_{rf} chosen to measure the lifetime. b) Atom number decays on the state $|2\rangle$ after the transfer for the detunings $\delta_{rf}/2\pi = 210$ and 350 Hz. The fits with exponential decays yield the lifetime of 1.85(5)s and 1.67(6)s, respectively, in good agreement with Table 1. For both figures, the error bars correspond to the rms uncertainties estimated over five experimental realizations.

with a numerical simulation for a repulsive disorder of amplitude $V_R/h = 416$ Hz. As said above, this excellent agreement is used to calibrate precisely the disorder amplitude in the experiments (with a 5% uncertainty).

Last, we study the scattering lifetime of the atoms transferred in the disorder-sensitive state $|2\rangle$ for the same configuration corresponding to $V_R/h = 416$ Hz. In order to maximize the signal-to-noise ratio, we choose two rf detuning, $\delta_{rf}/2\pi = 210$ Hz and 350 Hz, close to the maximum of the transfer curve $\Gamma(\delta_{rf})$. The decay of the atoms number (once the rf transfer field is switched off) is shown on Fig. 7b). The fits by exponential curves yield very similar lifetime of, respectively, $\tau_{210} = 1.85(5)$s and $\tau_{350} = 1.67(6)$s. These values are in very good agreement with the prediction in Table 1, thus validating our analysis. Most importantly, these values are larger than one second, which is crucial for our ongoing investigation of the Anderson transition.

5 Summary and outlook

In this paper, we have studied both theoretically and experimentally a new scheme to produce a 3D state-dependent disordered potential with a low spontaneous photon scattering rate in the disordered sensitive state. It is realized using a bichromatic speckle disorder whose properties have been investigated in details, in particular to quantify the conditions under which the two disordered potentials, created from two laser speckle field at two slightly different wavelengths, can cancel efficiently together for the insensitive state. Using this state-dependent disorder potential and a rf transfer from the insensitive state to the disorder-sensitive state, one can load ultracold atoms at a precise energy level in the disordered potential. The transferred atoms have a typical photon scattering lifetime on the second time scale, an improvement of two orders of magnitude compared to the monochromatic speckle scheme [20]. We therefore expect that scheme to allow us to effect precise measurements of the mobility edge and the critical exponents the 3D Anderson transition, whose precise determination remains an utmost experimental challenge [18].

It is worth noting that this scheme could be extended to other kind of optical potentials used to study disordered systems, such as those created by spatial light modulators as well as quasi-periodic lattices [4], see, e.g., [49,50]. It opens also many prospects to address fundamental questions related to the Anderson transition, such as the observation of multifractalilty [51], comparison with new theoretical approaches such as the one based on the "hidden landscape" [21,31], or general Anderson transition with different universality class [52], dimensions [53], or even in the presence of non-Hermitian disorder [54].

Acknowledgements The authors thank Vincent Denechaud and Adrien Signoles for early discussions and work. This work was supported by grant No. 601937 from the Simons Foundation and by an "Investissements

[4] While the general arguments exposed in Sect. 3.2 on the fundamental decorrelation of the potentials produced by two different wavelength would be essentially similar, each configuration would require specific calculations. A general analysis is, however, beyond the scope of this paper.

d'Avenir" grant from LabEx PALM (ANR-10-LABX-0039-PALM). A.A. acknowledges support through the Augustin Fresnel chair of the Institut d'Optique Graduate School, sponsored by Institut d'Optique and supported by Nokia Bell labs. He also acknowledges support from the iXcore-iXlife-IXblue foundation for research. V.V acknowledges support from Marie Skłodowska-Curie (Grant No. 655933)

Author contributions

All authors contributed equally to the paper.

Data Availability Statement This manuscript has no associated data or the data will not be deposited. [Authors' comment: The datasets generated during and/or analyze during the current study are available from the corresponding author under reasonable request.]

Declarations

Conflict of interest The authors declare that they have no conflict of interest.

Appendix A: Calculation of the bichromatic correlation function

A.1: Bichromatic correlation function of the diffuser

We extend the standard calculation of the diffuser correlation function to the bichromatic case. The laser's local phase fluctuations just after the diffuser is expressed as

$$\phi(\mathbf{r}_0) = 2\pi(n-1)\frac{\delta e(\mathbf{r}_0)}{\lambda} \tag{A1}$$

where the points $\mathbf{r}_0 = \{x_0, y_0, z = 0\}$ correspond to the diffuser's plane. $\delta e(\mathbf{r}_0)$ is the local fluctuation of the thickness of the diffuser, λ the laser wavelength and n stands for the glass index. Note that, within this definition, we don't consider the averaged phase transmission, that we set to $\overline{\phi} = 0$ for simplicity. Moreover, we assume the diffuser to have a Gaussian-distributed thickness with standard deviation σ_e, resulting in a phase standard deviation $\sigma_\phi = 2\pi(n-1)\sigma_e/\lambda$. The diffuser transmission is $t_{\text{diff}}(\mathbf{r}_0, \lambda) = e^{i\phi(\mathbf{r}_0)}$, and its ensemble average writes

$$\overline{t_{\text{diff}}} = \overline{e^{i\phi}} = \int \mathrm{d}\phi\, e^{i\phi}\, \mathcal{P}(\phi) = e^{-\sigma_\phi^2/2} \tag{A2}$$

with $\mathcal{P}(\phi) = 1/\sqrt{2\pi}\sigma_\phi \times \exp(-\phi^2/2\sigma_\phi^2)$.

The bichromatic correlation function of the diffuser is defined as

$$C_{\text{diff}}(\mathbf{r}_0, \mathbf{r}_0', \lambda_\text{p}, \lambda_\text{c}) = \overline{t_{\text{diff}}(\mathbf{r}_0, \lambda_\text{p}) t^*_{\text{diff}}(\mathbf{r}_0', \lambda_\text{c})}\,. \tag{A3}$$

Note that, the correlation function of the diffuser with a monochromatic illumination is obtained by merely setting $\lambda_\text{c} = \lambda_\text{p}$. Since the diffuser's thickness is a Gaussian random variable, the phase difference $\phi_\text{p}(\mathbf{r}_0) - \phi_\text{c}(\mathbf{r}_0')$ is a Gaussian variable as well and we can calculate as in equation (A2) to obtain

$$C_{\text{diff}}(\mathbf{r}_0, \mathbf{r}_0', \lambda_\text{p}, \lambda_\text{c}) = \overline{e^{i(\phi_\text{p}(\mathbf{r}_0) - \phi_\text{c}(\mathbf{r}_0'))}} \tag{A4}$$

$$= \exp\left[-2\pi^2(n-1)^2\sigma_\text{e}^2\left(\frac{1}{\lambda_\text{p}^2} + \frac{1}{\lambda_\text{c}^2}\right)\right] \times \exp\left[4\pi^2(n-1)^2\frac{2}{\lambda_\text{p}\lambda_\text{c}}\overline{\delta e(\mathbf{r}_0)\delta e(\mathbf{r}_0')}\right]. \tag{A5}$$

To characterize the granularity correlation function $\overline{\delta e(\mathbf{r}_0)\delta e(\mathbf{r}_0')}$ of the diffuser, we introduce r_e, which is the width of the thickness correlation function and describes the typical size of the transverse granularity of the diffuser's surface. By assuming a wide phase distribution $\sigma_\phi \gg 2\pi$ (equivalently $\sigma_\text{e} \gg \lambda$), the wave oscillates many times in a single granularity and the diffuser's thickness correlation function can be approximated by a bell-shaped curve:

$$\frac{\overline{\delta e(\mathbf{r}_0)\delta e(\mathbf{r}_0')}}{\sigma_\text{e}^2} \approx 1 - \frac{(\mathbf{r}_0 - \mathbf{r}_0')^2}{2r_\text{e}^2} \tag{A6}$$

when $|\mathbf{r}_0 - \mathbf{r}_0'| \ll r_\text{e}$. Finally, the bichromatic diffuser correlation function reads as

$$C_{\text{diff}}(\mathbf{r}_0, \mathbf{r}_0', \lambda_\text{p}, \lambda_\text{c}) = \exp\left(-\frac{\sigma_{\Delta\phi}^2}{2}\right) \times \exp\left(-\frac{(\mathbf{r}_0 - \mathbf{r}_0')^2}{2r_{\text{diff,p}}r_{\text{diff,c}}}\right) \tag{A7}$$

where $\sigma_{\Delta\phi}^2 = (\sigma_{\phi_\text{p}} - \sigma_{\phi_\text{c}})^2$ is the variance of the local phase difference $\Delta\phi(\mathbf{r}_0) = \phi_\text{p}(\mathbf{r}_0) - \phi_\text{c}(\mathbf{r}_0)$ and where we introduced the diffuser's phase correlation length $r_{\text{diff,p,c}} = r_\text{e}/\sigma_{\phi,p,c}$ (respectively, for the principal and compensating lasers).

A.2 Correlation function of the amplitude

We consider here the general two-point correlation function of bichromatic speckle field, at any positions $\mathbf{r}$ and $\mathbf{r}'$ and for different wavelengths λ_p and λ_c. Within the paraxial approximation, it is expressed as

$$\begin{aligned}\Gamma_{\mathcal{A}}(\mathbf{r},\mathbf{r}',\lambda_\mathrm{p},\lambda_\mathrm{c}) &= \overline{\mathcal{A}(\mathbf{r},\lambda_\mathrm{p})\mathcal{A}^*(\mathbf{r}',\lambda_\mathrm{c})} \\ &= \frac{e^{ik_\mathrm{p}\left(\overline{z}+\frac{x^2+y^2}{2\overline{z}}\right)}e^{-ik_\mathrm{c}\left(\overline{z}'+\frac{x'^2+y'^2}{2\overline{z}'}\right)}}{\lambda_\mathrm{p}\lambda_\mathrm{c}\overline{z}\overline{z}'} \\ &\times \int \mathrm{d}\mathbf{r}_0\mathrm{d}\mathbf{r}_0'\,\overline{t_\mathrm{diff}(\mathbf{r}_0,\lambda_\mathrm{p})t^*_\mathrm{diff}(\mathbf{r}_0',\lambda_\mathrm{c})} \\ &\times \mathcal{A}(\mathbf{r}_0,\lambda_\mathrm{p})\mathcal{A}^*(\mathbf{r}_0',\lambda_\mathrm{c}) \\ &\times e^{ik_\mathrm{p}\frac{\mathbf{r}_0^2}{2d_\mathrm{eff}}}e^{-ik_\mathrm{c}\frac{\mathbf{r}_0'^2}{2d'_\mathrm{eff}}}e^{-ik_\mathrm{p}\frac{\mathbf{r}\cdot\mathbf{r}_0}{\overline{z}}}e^{ik_\mathrm{c}\frac{\mathbf{r}'\cdot\mathbf{r}_0'}{\overline{z}'}} \end{aligned} \tag{A8}$$

where $\mathcal{A}(\mathbf{r}_0)$ is the amplitude just before the diffuser, and the ensemble average $\overline{\cdots}$ only acts on the transmissions t_diff. The effective distances d_eff are defined with respect to the focal plane by $1/d_\mathrm{eff} = 1/\overline{z} - 1/f$. Last, $\overline{z} = z + f$ is the longitudinal distance compared to the diffuser (z being the distance to the Fourier plane, see Fig. 4).

Using the change of variables $\{\mathbf{r}_0, \mathbf{r}_0'\} \to \{\mathbf{r}_{\mathrm{c},0} = (\mathbf{r}_0 + \mathbf{r}_0')/2,\ \Delta\mathbf{r}_0 = \mathbf{r}_0' - \mathbf{r}_0\}$, we obtain

$$\begin{aligned}\Gamma_{\mathcal{A}}(\mathbf{r},\mathbf{r}',\lambda_\mathrm{p},\lambda_\mathrm{p}) &\propto \frac{e^{ik_\mathrm{p}\left(\overline{z}+\frac{x^2+y^2}{2\overline{z}}\right)}e^{-ik_\mathrm{c}\left(\overline{z}'+\frac{x'^2+y'^2}{2\overline{z}'}\right)}}{\lambda_\mathrm{p}\lambda_\mathrm{c}\overline{z}\overline{z}'} \\ &\times \int \mathrm{d}\mathbf{r}_{\mathrm{c},0}\mathrm{d}\Delta\mathbf{r}_0\, C_\mathrm{diff}(\Delta\mathbf{r}_0,\lambda_\mathrm{p},\lambda_\mathrm{c}) \\ &\times \mathcal{A}(\mathbf{r}_{\mathrm{c},0}-\Delta\mathbf{r}_0/2,\lambda_\mathrm{p})\mathcal{A}^*(\mathbf{r}_{\mathrm{c},0}+\Delta\mathbf{r}_0/2,\lambda_\mathrm{c}) \\ &\times e^{i\mathbf{r}_{\mathrm{c},0}\cdot\left(\frac{k_\mathrm{c}\mathbf{r}'}{\overline{z}'}-\frac{k_\mathrm{p}\mathbf{r}}{\overline{z}}\right)}e^{i\frac{\Delta\mathbf{r}_0}{2}\cdot\left(\frac{k_\mathrm{p}\mathbf{r}}{\overline{z}}+\frac{k_\mathrm{c}\mathbf{r}'}{\overline{z}'}\right)}e^{i\frac{\mathbf{r}_{\mathrm{c},0}^2}{2}\left(\frac{k_\mathrm{p}}{d_\mathrm{eff}}-\frac{k_\mathrm{c}}{d'_\mathrm{eff}}\right)} \\ &\times e^{-i\frac{\Delta\mathbf{r}_0\cdot\mathbf{r}_{\mathrm{c},0}}{2}\left(\frac{k_\mathrm{p}}{d_\mathrm{eff}}+\frac{k_\mathrm{c}}{d'_\mathrm{eff}}\right)}e^{i\frac{\Delta\mathbf{r}_0^2}{8}\left(\frac{k_\mathrm{p}}{d_\mathrm{eff}}-\frac{k_\mathrm{c}}{d'_\mathrm{eff}}\right)}. \end{aligned} \tag{A9}$$

Let us now suppose that the typical size of the diffuser grains is small compared to the size of the incoming illumination $I(\mathbf{r}_0)$, meaning that on the size of C_diff, the incoming illumination is constant. Let us also suppose that the two incoming beams are in the same spatial mode: $\mathcal{A}(\mathbf{r}_0 - \Delta\mathbf{r}_0/2,\lambda_\mathrm{p})\mathcal{A}^*(\mathbf{r}_0 + \Delta\mathbf{r}_0/2,\lambda_\mathrm{c}) \approx \mathcal{A}(\mathbf{r}_0,\lambda_\mathrm{p})\mathcal{A}^*(\mathbf{r}_0,\lambda_\mathrm{c}) = I(\mathbf{r}_0)$ (for simplicity, we discard from now the c subscript from $\mathbf{r}_{\mathrm{c},0}$). We find

$$\begin{aligned}\Gamma_{\mathcal{A}}(\mathbf{r},\mathbf{r}',\lambda_\mathrm{p},\lambda_\mathrm{c}) &= \frac{e^{ik_\mathrm{p}\left(\overline{z}+\frac{x^2+y^2}{2\overline{z}}\right)}e^{-ik_\mathrm{c}\left(\overline{z}'+\frac{x'^2+y'^2}{2\overline{z}'}\right)}}{\lambda_\mathrm{p}\lambda_\mathrm{c}\overline{z}\overline{z}'} \\ &\times \int \mathrm{d}\mathbf{r}_0\, I(\mathbf{r}_0)e^{i\frac{\mathbf{r}_0^2}{2}\left(\frac{k_\mathrm{p}}{d_\mathrm{eff}}-\frac{k_\mathrm{c}}{d'_\mathrm{eff}}\right)}e^{i\mathbf{r}_0\cdot\left(\frac{k_\mathrm{c}\mathbf{r}'}{\overline{z}'}-\frac{k_\mathrm{p}\mathbf{r}}{\overline{z}}\right)} \\ &\times \int \mathrm{d}\Delta\mathbf{r}_0\, C_\mathrm{diff}(\Delta\mathbf{r}_0,\lambda_\mathrm{p},\lambda_\mathrm{c})\, e^{-i\frac{\Delta\mathbf{r}_0\cdot\mathbf{r}_0}{2}\left(\frac{k_\mathrm{p}}{d_\mathrm{eff}}+\frac{k_\mathrm{c}}{d'_\mathrm{eff}}\right)} \\ &\times e^{i\frac{\Delta\mathbf{r}_0}{2}\cdot\left(\frac{k_\mathrm{p}\mathbf{r}}{\overline{z}}+\frac{k_\mathrm{c}\mathbf{r}'}{\overline{z}'}\right)}. \end{aligned} \tag{A10}$$

A.3 3D monochromatic correlation close to the Fourier plane

In this part, we give the explicit calculation of the *spatial* autocorrelation function of a monochromatic laser speckle field, i.e., at two different points $\mathbf{r}, \mathbf{r}'$ but at the same wavelength $\lambda_\mathrm{p} = \lambda_\mathrm{c} = \lambda$. Such derivation is very well known [37] but it will be used for the derivation of the bichromatic correlation function in a simple form, which is an important result of the paper. The two-point autocorrelation function is defined as

$$c_\mathrm{3D}(\Delta\mathbf{r}_\perp,\Delta z) = \frac{\overline{\delta I(\mathbf{r}_\perp+\Delta\mathbf{r}_\perp, z+\Delta z)\delta I(\mathbf{r}_\perp, z)}}{\overline{\delta I^2}} \tag{A11}$$

with $\mathbf{r}_\perp = \{x, y\}$. Close to the Fourier plane and to the optical axis, the numerator reads as $\overline{\delta I(\Delta\mathbf{r}_\perp,\Delta z)\delta I(\mathbf{0},0)}$ and is computed using Wick's theorem:

$$\begin{aligned}\overline{\delta I(\Delta\mathbf{r}_\perp,\Delta z)\delta I(\mathbf{0},0)} &= |\Gamma_{\mathcal{A}}(\Delta\mathbf{r}_\perp,\Delta z)|^2 \\ &= \left|\overline{\mathcal{A}(\Delta\mathbf{r}_\perp,\Delta z)\mathcal{A}^*(\mathbf{0},0)}\right|^2 \\ &= \left|\frac{1}{\lambda^2 f^2}\int \mathrm{d}\mathbf{r}_0\, I(\mathbf{r}_0)\, e^{-i\frac{\mathbf{r}_0^2 k\Delta z}{2f^2}}\, e^{-i\frac{k\mathbf{r}_0\cdot\Delta\mathbf{r}_\perp}{f}}\right. \\ &\times \left.\int \mathrm{d}\Delta\mathbf{r}_0\, C_\mathrm{diff}(\Delta\mathbf{r}_0)\, e^{i\frac{\Delta\mathbf{r}_0\cdot\mathbf{r}_0 k\Delta z}{2f^2}}\, e^{i\frac{k\Delta\mathbf{r}_0\cdot\Delta\mathbf{r}_\perp}{2f}}\right|^2. \end{aligned} \tag{A12}$$

By comparing the different phase terms, we can neglect the exponentials of the second integral. After normalization by $|\overline{I(\mathbf{0},0)}|^2$, and identifying a Fourier transform, we obtain the usual result [37]:

$$c_\mathrm{3D}(\Delta\mathbf{r}_\perp,\Delta z) = \frac{\left|\mathrm{FT}\left[I(\mathbf{r}_0)\, e^{-i\frac{\mathbf{r}_0^2 k\Delta z}{2f^2}}\right]_{\frac{k\Delta\mathbf{r}_\perp}{f}}\right|^2}{\left|\int \mathrm{d}\mathbf{r}_0\, I(\mathbf{r}_0)\right|^2}. \tag{A13}$$

A.4 Bichromatic correlation function of the speckle

We consider now bichromatic correlation function $c_{2\lambda}(\mathbf{r}_\perp, z, \lambda_\mathrm{p}, \lambda_\mathrm{c})$ between two speckle fields created at different wavelength speckle pattern *at a single point* located by $\mathbf{r} = \{\mathbf{r}_\perp, z\}$ compared to the center of the Fourier plane. As discussed in the text, the correlation between the two speckles disorder potentials is directly linked to this function, see Eq. (10). It is defined as

$$c_{2\lambda}(\mathbf{r}_\perp, z, \lambda_\mathrm{p}, \lambda_\mathrm{c}) = \frac{\overline{\delta I(\mathbf{r}_\perp, z, \lambda_\mathrm{p})\delta I(\mathbf{r}_\perp, z, \lambda_\mathrm{c})}}{\overline{I(\mathbf{r}_\perp, z, \lambda_\mathrm{p})}\,\overline{I(\mathbf{r}_\perp, z, \lambda_\mathrm{c})}}. \tag{A14}$$

The correlation function in the numerator is computed using Wick's theorem $\overline{\delta I(\mathbf{r}_\perp, z, \lambda_\mathrm{p})\delta I(\mathbf{r}_\perp, z, \lambda_\mathrm{c})}$

$= |\Gamma_{\mathcal{A}}(\mathbf{r}_\perp, z, \lambda_\mathrm{p}, \lambda_\mathrm{c})|^2$, with

$$
\begin{aligned}
|\Gamma_{\mathcal{A}}(\mathbf{r}_\perp, z, \lambda_\mathrm{p}, \lambda_\mathrm{c})|^2 &= \left|\overline{\mathcal{A}(\mathbf{r}_\perp, z, \lambda_\mathrm{p}) \mathcal{A}^*(\mathbf{r}_\perp, z, \lambda_\mathrm{c})}\right|^2 \\
&= \left| \frac{1}{\lambda_\mathrm{p}\lambda_\mathrm{c} z^2} \int \mathrm{d}\mathbf{r}_0 \, I(\mathbf{r}_0) \, e^{-i\frac{\mathbf{r}_0^2 z}{2f^2}(k_\mathrm{p}-k_\mathrm{c})} \right. \\
&\quad \times e^{i\frac{\mathbf{r}_\perp \cdot \mathbf{r}_0}{f}(k_\mathrm{c}-k_\mathrm{p})} \int \mathrm{d}\Delta\mathbf{r}_0 \, C_\mathrm{diff}(\Delta\mathbf{r}_0, \lambda_\mathrm{p}, \lambda_\mathrm{c}) \\
&\quad \left. \times \, e^{i\frac{\Delta\mathbf{r}_0 \cdot \mathbf{r}_0 z}{f^2}\frac{k_\mathrm{p}+k_\mathrm{c}}{2}} \, e^{i\frac{\Delta\mathbf{r}_0 \cdot \mathbf{r}_\perp}{f}\frac{k_\mathrm{p}+k_\mathrm{c}}{2}} \right|^2 . \qquad \text{(A15)}
\end{aligned}
$$

Using (i) the same approximation as in Eq. (A12) for the phase exponentials of the second integral, (ii) the normalization by the average intensity profile around the center $|\overline{I(\mathbf{0}, 0)}|^2$, and (iii) $\delta\lambda = |\lambda_\mathrm{c} - \lambda_\mathrm{p}| \ll \lambda_{\mathrm{p,c}} \sim \lambda$, we obtain

$$
\begin{aligned}
&c_{2\lambda}(\mathbf{r}_\perp, z, \lambda_\mathrm{p}, \lambda_\mathrm{c}) \\
&= \frac{\left| \int \mathrm{d}\Delta\mathbf{r}_0 \, C_\mathrm{diff}(\Delta\mathbf{r}_0, \lambda_\mathrm{p}, \lambda_\mathrm{c}) \right|^2}{\int \mathrm{d}\Delta\mathbf{r}_0 \, C_\mathrm{diff}(\Delta\mathbf{r}_0, \lambda_\mathrm{p}) \int \mathrm{d}\Delta\mathbf{r}_0 \, C_\mathrm{diff}(\Delta\mathbf{r}_0, \lambda_\mathrm{c})} \\
&\times \frac{\left| \int \mathrm{d}\mathbf{r}_0 \, I(\mathbf{r}_0) \, e^{-ik\frac{\mathbf{r}_0^2 z}{2f^2}\frac{\delta\lambda}{\lambda}} \, e^{ik\frac{\mathbf{r}_\perp \cdot \mathbf{r}_0}{f}\frac{\delta\lambda}{\lambda}} \right|^2}{\left| \int \mathrm{d}\mathbf{r}_0 \, I(\mathbf{r}_0) \right|^2} \qquad \text{(A16)}
\end{aligned}
$$

and consists of two terms. The first one only features the diffuser, while the second describes the free space propagation after the diffuser. The first term can be computed using

$$
\int \mathrm{d}\Delta\mathbf{r}_0 \, C_\mathrm{diff}(\Delta\mathbf{r}_0, \lambda) = 2\pi r_\mathrm{diff}^2 \qquad \text{(A17)}
$$

The normalized bichromatic correlation function finally reads as

$$
\begin{aligned}
&c_{2\lambda}(\mathbf{r}_\perp, z, \lambda_\mathrm{p}, \lambda_\mathrm{c}) \\
&= C_\mathrm{diff}^2(\mathbf{0}, \lambda_\mathrm{p}, \lambda_\mathrm{c}) \frac{\left| \mathrm{FT}\left[I(\mathbf{r}_0) \, e^{-ik\frac{\mathbf{r}_0^2 z}{2f^2}} \right]_{k\frac{\mathbf{r}_\perp}{f}\frac{\delta\lambda}{\lambda}} \right|^2}{\left| \int \mathrm{d}\mathbf{r}_0 \, I(\mathbf{r}_0) \right|^2} \\
&= e^{-\sigma_{\Delta\phi}^2} \, c_\mathrm{3D}\left(\mathbf{r}_\perp \frac{\delta\lambda}{\lambda}, z\frac{\delta\lambda}{\lambda} \right) \qquad \text{(A18)}
\end{aligned}
$$

References

1. I. Bloch, J. Dalibard, W. Zwerger, Many-body physics with ultracold gases. Rev. Mod. Phys. **80**, 885–964 (2008)
2. J. Billy, V. Josse, Z. Zuo, A. Bernard, B. Hambrecht, P. Lugan, D. Clément, L. Sanchez-Palencia, P. Bouyer, A. Aspect, Direct observation of anderson localization of matter waves in a controlled disorder. Nature **453**, 891–894 (2008). https://doi.org/10.1038/nature07000
3. G. Roati, C. D'Errico, L. Fallani, M. Fattori, C. Fort, M. Zaccanti, G. Modugno, M. Modugno, M. Inguscio, Anderson localization of a non-interacting bose-einstein condensate. Nature **453**, 895–898 (2008). https://doi.org/10.1038/nature07071
4. F. Jendrzejewski, K. Müller, J. Richard, A. Date, T. Plisson, P. Bouyer, A. Aspect, V. Josse, Coherent backscattering of ultracold atoms. Phys. Rev. Lett. **109**, 195–302 (2012). https://doi.org/10.1103/PhysRevLett.109.195302
5. K. Müller, J. Richard, V.V. Volchkov, V. Denechaud, P. Bouyer, A. Aspect, V. Josse, Suppression and revival of weak localization through control of time-reversal symmetry. Phys. Rev. Lett. **114**, 205–301 (2015). https://doi.org/10.1103/PhysRevLett.114.205301
6. S.S. Kondov, W.R. McGehee, J.J. Zirbel, B. DeMarco, Three-dimensional anderson localization of ultracold matter. Science **334**(6052), 66–68 (2011)
7. F. Jendrzejewski, A. Bernard, K. Müller, P. Cheinet, V. Josse, M. Piraud, L. Pezzé, L. Sanchez-Palencia, A. Aspect, P. Bouyer, Three-dimensional localization of ultracold atoms in an optical disordered potential. Nat. Phys. **8**, 398–403 (2012). https://doi.org/10.1038/nphys2256
8. G. Semeghini, M. Landini, P. Castilho, S. Roy, G. Spagnolli, A. Trenkwalder, M. Fattori, M. Inguscio, G. Modugno, Measurement of the mobility edge for 3d anderson localization. Nat. Phys. **11**, 554–559 (2015). https://doi.org/10.1038/nphys3339
9. L. Sanchez-Palencia, D. Clément, P. Lugan, P. Bouyer, G.V. Shlyapnikov, A. Aspect, Anderson localization of expanding Bose-Einstein condensates in random potentials. Phys. Rev. Lett. **98**, 210–401 (2007). https://doi.org/10.1103/PhysRevLett.98.210401
10. N. Cherroret, T. Karpiuk, C.A. Müller, B. Grémaud, C. Miniatura, Coherent backscattering of ultracold matter waves: Momentum space signatures. Phys. Rev. A **85**, 011604 (2012). https://doi.org/10.1103/PhysRevA.85.011604
11. E. Abrahams, P.W. Anderson, D.C. Licciardello, T.V. Ramakrishnan, Scaling theory of localization: absence of quantum diffusion in two dimensions. Phys. Rev. Lett. **42**, 673–676 (1979). https://doi.org/10.1103/PhysRevLett.42.673
12. F. Evers, A.D. Mirlin, Anderson transitions. Rev. Mod. Phys. **80**, 1355–1417 (2008). https://doi.org/10.1103/RevModPhys.80.1355
13. R.C. Kuhn, O. Sigwarth, C. Miniatura, D. Delande, C.A. Müller, Coherent matter wave transport in speckle potentials. New J. Phys. **9**(6), 161–161 (2007). https://doi.org/10.1088/1367-2630/9/6/161
14. S.E. Skipetrov, A. Minguzzi, B.A. van Tiggelen, B. Shapiro, Anderson localization of a Bose-Einstein condensate in a 3d random potential. Phys. Rev. Lett. **100**, 165301 (2008). https://doi.org/10.1103/PhysRevLett.100.165301
15. M. Piraud, L. Pezzé, L. Sanchez-Palencia, Quantum transport of atomic matter waves in anisotropic two-

dimensional and three-dimensional disorder. New J. Phys. **15**(7), 075007 (2013). https://doi.org/10.1088/1367-2630/15/7/075007
16. M. Piraud, L. Sanchez-Palencia, B. van Tiggelen, Anderson localization of matter waves in three-dimensional anisotropic disordered potentials. Phys. Rev. A **90**, 063639 (2014). https://doi.org/10.1103/PhysRevA.90.063639
17. D. Delande, G. Orso, Mobility edge for cold atoms in laser speckle potentials. Phys. Rev. Lett. **113**, 060601 (2014). https://doi.org/10.1103/PhysRevLett.113.060601
18. M. Pasek, G. Orso, D. Delande, Anderson localization of ultracold atoms: Where is the mobility edge? Phys. Rev. Lett. **118**, 170403 (2017). https://doi.org/10.1103/PhysRevLett.118.170403
19. K. Slevin, T. Ohtsuki, Critical exponent for the Anderson transition in the three-dimensional orthogonal universality class. New J. Phys. **16**(1), 015012 (2014). https://doi.org/10.1088/1367-2630/16/1/015012
20. V.V. Volchkov, M. Pasek, V. Denechaud, M. Mukhtar, A. Aspect, D. Delande, V. Josse, Measurement of spectral functions of ultracold atoms in disordered potentials. Phys. Rev. Lett. **120**, 060404 (2018). https://doi.org/10.1103/PhysRevLett.120.060404
21. M. Filoche, S. Mayboroda, Universal mechanism for anderson and weak localization. Proc. Natl. Acad. Sci. **109**(37), 14761–14766 (2012)
22. T. Karpiuk, N. Cherroret, K.L. Lee, B. Grémaud, C.A. Müller, C. Miniatura, Coherent forward scattering peak induced by Anderson localization. Phys. Rev. Lett. **109**, 190601 (2012). https://doi.org/10.1103/PhysRevLett.109.190601
23. T. Micklitz, C.A. Müller, A. Altland, Echo spectroscopy of anderson localization. Phys. Rev. B **91**, 064203 (2015). https://doi.org/10.1103/PhysRevB.91.064203
24. S. Ghosh, C. Miniatura, N. Cherroret, D. Delande, Coherent forward scattering as a signature of Anderson metal-insulator transitions. Phys. Rev. A **95**, 041602 (2017). https://doi.org/10.1103/PhysRevA.95.041602
25. C. Hainaut, I. Manai, J.F. Clément, J.C. Garreau, P. Szriftgiser, G. Lemarié, N. Cherroret, D. Delande, R. Chicireanu, Controlling symmetry and localization with an artificial gauge field in a disordered quantum system. Nat. Commun. **9**(1), 1382 (2018). https://doi.org/10.1038/s41467-018-03481-9
26. M. Martinez, G. Lemarié, B. Georgeot, C. Miniatura, O. Giraud, Coherent forward scattering peak and multifractality. Phys. Rev. Res. **3**, L032044 (2021). https://doi.org/10.1103/PhysRevResearch.3.L032044
27. D.H. White, T.A. Haase, D.J. Brown, M.D. Hoogerland, M.S. Najafabadi, J.L. Helm, C. Gies, D. Schumayer, D.A.W. Hutchinson, Observation of two-dimensional anderson localisation of ultracold atoms. Nat. Commun. **11**(1), 4942 (2020). https://doi.org/10.1038/s41467-020-18652-w
28. G. Orso, Anderson transition of cold atoms with synthetic spin-orbit coupling in two-dimensional speckle potentials. Phys. Rev. Lett. **118**, 105301 (2017). https://doi.org/10.1103/PhysRevLett.118.105301. https://link.aps.org/doi/10.1103/PhysRevLett.118.105301
29. M.I. Trappe, D. Delande, C.A. Müller, Semiclassical spectral function for matter waves in random potentials. J. Phys. A Math. Theoret. **48**(24), 245102 (2015). https://doi.org/10.1088/1751-8113/48/24/245102
30. T. Prat, N. Cherroret, D. Delande, Semiclassical spectral function and density of states in speckle potentials. Phys. Rev. A **94**, 022114 (2016). https://doi.org/10.1103/PhysRevA.94.022114
31. P. Pelletier, D. Delande, V. Josse, A. Aspect, S. Mayboroda, D.N. Arnold, M. Filoche, Spectral functions and localization-landscape theory in speckle potentials. Phys. Rev. A **105**, 023314 (2022). https://doi.org/10.1103/PhysRevA.105.023314
32. I.H. Deutsch, P.S. Jessen, Quantum-state control in optical lattices. Phys. Rev. A **57**, 1972–1986 (1998). https://doi.org/10.1103/PhysRevA.57.1972
33. O. Mandel, M. Greiner, A. Widera, T. Rom, T.W. Hänsch, I. Bloch, Coherent transport of neutral atoms in spin-dependent optical lattice potentials. Phys. Rev. Lett. **91**, 010407 (2003). https://doi.org/10.1103/PhysRevLett.91.010407
34. B. Gadway, D. Pertot, R. Reimann, D. Schneble, Superfluidity of interacting bosonic mixtures in optical lattices. Phys. Rev. Lett. **105**, 045303 (2010). https://doi.org/10.1103/PhysRevLett.105.045303
35. R. Grimm, M. Weidemüller, Y.B. Ovchinnikov, (Academic Press, 2000), pp. 95–170. https://doi.org/10.1016/S1049-250X(08)60186-X
36. J. Richard, L.K. Lim, V. Denechaud, V.V. Volchkov, B. Lecoutre, M. Mukhtar, F. Jendrzejewski, A. Aspect, A. Signoles, L. Sanchez-Palencia, V. Josse, Elastic scattering time of matter waves in disordered potentials. Phys. Rev. Lett. **122**, 100403 (2019). https://doi.org/10.1103/PhysRevLett.122.100403
37. J.W. Goodman, *Speckle Phenomena in Optics: Theory and Applications* (Roberts and Company, 2007)
38. R.C. Kuhn, O. Sigwarth, C. Miniatura, D. Delande, C.A. Müller, Coherent matter wave transport in speckle potentials. New J. Phys. **9**(6), 161–161 (2007). https://doi.org/10.1088/1367-2630/9/6/161
39. B. Shapiro, Cold atoms in the presence of disorder. J. Phys. A Math. Theoret. **45**(14), 143001 (2012). https://doi.org/10.1088/1751-8113/45/14/143001
40. A. Signoles, B. Lecoutre, J. Richard, L.K. Lim, V. Denechaud, V.V. Volchkov, V. Angelopoulou, F. Jendrzejewski, A. Aspect, L. Sanchez-Palencia, V. Josse, Ultracold atoms in disordered potentials: elastic scattering time in the strong scattering regime. New J. Phys. **21**(10), 105002 (2019). https://doi.org/10.1088/1367-2630/ab466f
41. M. Born, E. Wolf, A.B. Bhatia, P.C. Clemmow, D. Gabor, A.R. Stokes, A.M. Taylor, P.A. Wayman, W.L. Wilcock, *Principles of Optics: Electromagnetic Theory of Propagation, Interference and Diffraction of Light*, 7th edn. (Cambridge University Press, 1999). https://doi.org/10.1017/CBO9781139644181
42. B. Lecoutre, Transport quantique d'atomes ultra-froids en milieu désordonné : Temps de diffusion élastique et fonctions spectrales. Theses, Université Paris-Saclay (2020). https://pastel.archives-ouvertes.fr/tel-03141534
43. J. Richard, Propagation d'atomes ultra-froids en milieu désordonné - Étude dans l'espace des impulsions de phénomènes de diffusion et de localisation. Theses, Uni-

versité Paris Saclay (COmUE) (2015). https://pastel.archives-ouvertes.fr/tel-01246561
44. Supplemental material of J. Richard *et al.* Phys. Rev. Lett. **122**, 100403 (2019). https://journals.aps.org/prl/supplemental/10.1103/PhysRevLett.122.100403
45. H.J. Lewandowski, D.M. Harber, D.L. Whitaker, E.A. Cornell, Observation of anomalous spin-state segregation in a trapped ultracold vapor. Phys. Rev. Lett. **88**, 070403 (2002). https://doi.org/10.1103/PhysRevLett.88.070403
46. D.A. Steck, Rubidium 87 d line data (2001). https://www.blogs.uni-mainz.de/fpraktikumphysik/files/2022/05/V65_Rubidium.pdf
47. L. Sanchez-Palencia, Smoothing effect and delocalization of interacting Bose-Einstein condensates in random potentials. Phys. Rev. A **74**, 053625 (2006). https://doi.org/10.1103/PhysRevA.74.053625
48. Supplemental material of V. Volchkov *et al.* Phys. Rev. Lett. **120**, 060404 (2018). https://journals.aps.org/prl/supplemental/10.1103/PhysRevLett.120.060404
49. G. Roati, C. D'Errico, L. Fallani, M. Fattori, C. Fort, M. Zaccanti, G. Modugno, M. Modugno, M. Inguscio, Anderson localization of a non-interacting Bose-Einstein condensate. Nature **453**(7197), 895–898 (2008). https://doi.org/10.1038/nature07071
50. J.Y. Choi, S. Hild, J. Zeiher, P. Schauß, A. Rubio-Abadal, T. Yefsah, V. Khemani, D.A. Huse, I. Bloch, C. Gross, Exploring the many-body localization transition in two dimensions. Science **352**(6293), 1547–1552 (2016). https://doi.org/10.1126/science.aaf8834
51. M.A. Werner, E. Demler, A. Aspect, G. Zaránd, Selective state spectroscopy and multifractality in disordered Bose-Einstein condensates: a numerical study. Sci. Rep. **8**(1), 3641 (2018). https://doi.org/10.1038/s41598-018-21870-4
52. T. Wang, T. Ohtsuki, R. Shindou, Universality classes of the Anderson transition in the three-dimensional symmetry classes aiii, bdi, c, d, and ci. Phys. Rev. B **104**, 014206 (2021). https://doi.org/10.1103/PhysRevB.104.014206
53. G. Orso, Anderson transition of cold atoms with synthetic spin-orbit coupling in two-dimensional speckle potentials. Phys. Rev. Lett. **118**, 105301 (2017). https://doi.org/10.1103/PhysRevLett.118.105301
54. X. Luo, T. Ohtsuki, R. Shindou, Universality classes of the Anderson transitions driven by non-Hermitian disorder. Phys. Rev. Lett. **126**, 090402 (2021). https://doi.org/10.1103/PhysRevLett.126.090402